

# Revisiting Temperature and Magnetic Effects on the Fe-30 Wt Pct Ni Martensite Transformation Curve



J.R.C. GUIMARÃES and P.R. RIOS

This work revisits the relationship between the volume fraction of martensite and the transformed microstructure. This relationship is analyzed by considering that although thermodynamic principles determine the possibility of transformation, the size and arrangement of the martensite units over the austenite grains is determined by the local surroundings. The proposed equation for the transformation curve incorporates the probabilistic aspect of the initial transformation in a limited number of scattered austenite grains and autocatalysis. The validation of the model, already verified with data typical of FeC steels, FeNiC and FeNiMn alloys, is extended in this study to a transformation that exhibits microstructure diversity. Finally, we show that the model fits the transformation curves typical of “18Cr-8Ni” stainless steel; this finding demonstrates that the model is applicable to transformation curves characteristic of other systems due to a conceptualization based on the intrinsic aspects of martensite transformation in steels.

<https://doi.org/10.1007/s11661-018-4943-2>

© The Minerals, Metals & Materials Society and ASM International 2018

## I. INTRODUCTION

THE martensite transformation curve, which expresses the volume fraction transformed vs an external variable, is an expeditious tool to select a steel and its treatment to fit an engineering purpose. Historically, the martensite transformation curves have been described by empirical equations with coefficients that referred to the steel composition.<sup>[1,2]</sup> Moreover, such equations assumed athermal (time-independent, nonthermally activated) kinetics. The isothermal (thermally activated and time-dependent) transformation and the mechanically induced ones were acknowledged considerably later. Meantime, microstructure and thermodynamic aspects were formally introduced in descriptions of the transformation curve,<sup>[3–11]</sup> and athermal and isothermal aspects have been acknowledged in steels transformed by continuously cooling.<sup>[12–14]</sup> The renewed interest in the description of the martensite transformation curves (the topic of the present work) stems from the fact that

martensite has become a means to optimize engineering steels.

## II. BACKGROUND

In a previous paper,<sup>[15]</sup> we introduced a formalism to describe the martensite transformation curve observed in steels, considering generally accepted aspects of such transformation (diffusionless, autocatalytic, nucleation-controlled, and displacive) with progress that is also influenced by the environment where the units form.<sup>[16]</sup> The formalism has been validated with library data pertaining to a bursting FeNiC alloy,<sup>[17]</sup> low-carbon steels,<sup>[7]</sup> and in a FeNiMn alloy that transforms isothermally.<sup>[18]</sup> Further to describing transformation curves with very high fitting correlations, the parameters of the model expeditiously relate to kinetic aspects of the transformation. In this study, we extend the validation by considering the martensite transformation in Fe-30wt pctNi, which exhibits microstructural diversity.<sup>[19,20]</sup>

## III. FORMALISM

The early work by Cech and Turnbull<sup>[21]</sup> demonstrated that in particulate materials, the martensite transformation initiates heterogeneously at limited and randomly distributed particles such that the probability that a particle contains at least one nucleation locus at temperature  $T$ , which may be expressed as<sup>[22]</sup>

---

J.R.C. GUIMARÃES is with the Universidade Federal Fluminense, Escola de Engenharia Industrial Metalúrgica de Volta Redonda, Volta Redonda, RJ 27255-125, Brazil and also with the Mal.Moura 338H/22C, São Paulo, SP 05641-000, Brazil. P.R. RIOS is with the Universidade Federal Fluminense, Escola de Engenharia Industrial Metalúrgica de Volta Redonda. Contact e-mail: prrios@id.uff.br

Manuscript submitted May 1, 2018.

Article published online October 3, 2018

$$P_p = 1 - \exp(-q_p n_V^T), \quad [1]$$

where  $n_V^T$  is the number density of nucleation sites at temperature  $T$  and  $q_p$  is the mean particle volume. Of course, any grain that has at least one operational nucleation locus at temperature  $T$  will be partially transformed as a primary plate arises at each nucleation site. Therefore, the above probability is equivalent to the volume fraction of partially transformed grains,  $V_{VG}$ .

The scarcity and randomness of the initial nucleation sites also underlies the transformation in polycrystalline materials. However, intergrain interaction—martensite units transforming a grain may induce the transformation in an adjacent one—yields clusters of transformed grains.<sup>[17]</sup> Based on results of computer simulation, Guimarães and Saavedra<sup>[23]</sup> described this autocatalytic spread of martensite by a heuristic equation:

$$V_{VG} = 1 - \exp(-qN_{VM}/\beta), \quad [2]$$

where  $q$  is the mean austenite grain volume,  $N_{VM}$  is the total number of units transformed, and  $\beta$  is the mean number of units per partially transformed grains. Eq. [2] shows that the number density of transformed grains in such a process is  $N_{VG} = N_{VM}/\beta$ .

Proceeding to calculate the martensite volume fraction transformed,  $V_{VM}$ , note that the transformation follows a “spread and fill-in” course,<sup>[24]</sup> where the spread depends on martensite nucleation in untransformed grains and the fill-in results from intragrain autocatalysis. Therefore, considering the probabilistic aspect of the initial transformation, we express the probability of finding martensite in the material by the product of the number density of transformed grains,  $N_{VG}$ , times the volume of martensite per grain:  $P_M = N_{VG} \cdot v_{ML} \cdot \beta$ , where  $v_{ML}$  is the mean volume and  $\beta$  is the average number of martensite units in the transformed grains. Substituting  $N_{VG} = N_{VM}/\beta$  gives  $P_M = v_{ML}N_{VM}$ . Bearing in mind the randomness of the transformation,<sup>[21,22]</sup> we express the overall volume fraction transformed, tantamount to the probability of finding martensite in the material, as

$$V_{VM} = 1 - \exp(-v_{ML}N_{VM}). \quad [3]$$

Note that  $v_{ML}$  reflects the influences from size limitation and from the relaxation of transformation strains by mutual accommodation and/or plastic deformation. Therefore,  $v_{ML}$  varies with the local reaction environment.

To introduce the external variable,  $\xi$ , into Eq. [3] and obtain an equation for the transformation curve, we related  $N_{VM}$  and  $\xi$  by means of a power-law compatible with the autocatalysis, as performed by Huyan *et al.*<sup>[9]</sup> to express martensite fraction to the transformation driving force. In differential form,

$$dN_{VM} = \varphi^K N_{VM} \frac{d\xi}{\xi}, \quad [4]$$

where  $\varphi^K$  is a kinetic factor. Integrating Eq. [4] and substituting into Eq. [3] gives

$$V_{VM} = 1 - \exp\left(-V_{VM0} \left(\frac{\xi - \xi^*}{\xi_0 - \xi^*}\right)^{\varphi^K}\right), \quad [5]$$

where  $\xi_0$  is an operational estimate of  $\xi^*$  and  $V_{VM0} = v_{ML}N_{VM0}$  is the volume fraction transformed at  $\xi_0$ . The integration of Eq. [5] has been worked out in Reference 15. In the case of athermal (time-independent) transformation,  $\xi^*$  equals the highest temperature at which an austenite defect is able to sustain correlated atomic groups in the presence of thermal agitation ( $T^*$ ) and  $\xi_0$  equals the martensite-start temperature ( $M_s$ ). Since athermal martensite occurs upon decreasing the temperature, substituting into Eq. [5]:  $-dT$  for  $d\xi$ , and  $(T^* - T)$  for  $(\xi - \xi_0)$  yields

$$V_{VM} = 1 - \exp\left(-V_{VM0} \left(\frac{T^* - T}{T^* - M_s}\right)^{\varphi^K}\right). \quad [6]$$

In the case of a thermally activated (time-dependent, isothermal) transformation, we substitute the incubation factor  $\tau$  for  $\xi^*$  and the operational reference time ( $t_0$ ) for  $\xi_0$ ,

$$V_{VM} = 1 - \exp\left(-V_{VM0} \left(\frac{t - \tau}{t_0 - \tau}\right)^{\varphi^K}\right). \quad [7]$$

Fitting an experimental transformation curve to Eqs. [6] or [7] yields descriptors of the transformation kinetics ( $\tau$  and  $\varphi^K$ ), as well as of initial transformation in the grains ( $V_{VM0}$ ). Notably, the model is generally applicable to steels because Eq. [5] acknowledges the influence of intrinsic aspects of the transformation related to the microstructure development and thus to the volume fraction transformed.

#### IV. VALIDATION AND ANALYSIS OF DATA AND PARAMETERS

As in previous studies, we used data from an independent worker to check the model. Figure 1 shows

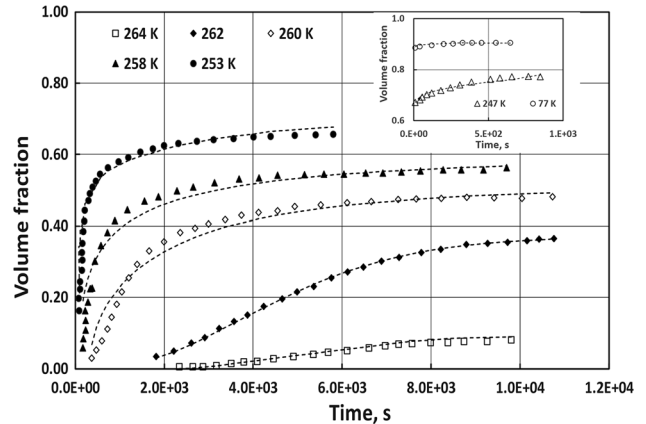


Fig. 1—Martensite transformation curves. The markings show the incorporated data from Ref. [20]. The dashed lines show the fitting with the model Eq. [7].

the transformation curves typical of the Fe-29.6 wt pct Ni alloy depicted in Figure 9 of Korenko's book.<sup>[20]</sup> For the sake of brevity, we will skip the description of the procedures followed by the author. However, it is worth mentioning that we incorporated his data by repeatedly ( $\times 3$ ) scanning and digitizing the charts in that book. Noting that the original charts did not have error bars; we estimate the errors at about  $\pm 5$  pct based on our experience with the quantitative metallographic methods used.

A parametric least-squares procedure was used to fit the data (symbols) with Eq. [7], yielding the dashed lines in Figure 1. The values of the fitting parameters,  $\phi^K$ ,  $\tau$ , and  $V_{VM0}$ , as well as the fitting correlations, are shown in Table I. At the higher transformation temperatures, the transformation is time-dependent. However, at the lower temperatures, the transformation accelerates, and eventually, an initial transformation burst precedes time-dependent tails, which flatten at volume fractions less than unity. However, the overall fraction transformed (burst + tail) increases with decreasing reaction temperature.

Note in Figure 2 that between 264 K and 253 K, the Arrhenius equation describes the temperature dependences in  $\phi^K$ , as well as in  $\tau$ . The similar slopes suggest similar thermally activated mechanisms along the transformation course. Note also that below 253 K,  $\phi^K$  becomes nearly temperature-invariant, whereas  $\tau$  continues to follow the Arrhenius equation.

The martensite transformation in Fe-29.6 wt pct Ni as in several other alloys and steels is autocatalytic.<sup>[25,26]</sup> However, the Fe-29.6 wt pct Ni martensite exhibits microstructure diversity characterized by the formation of laths or twinned plates, depending on the transformation temperature. The former are observed at high transformation temperatures, whereas the latter predominate at the lower temperatures.<sup>[19,20]</sup> This microstructure diversity in the Fe-Ni alloys has been attributed to invar strengthening of the austenite<sup>[27]</sup> and/or to the mobility of the martensite interface.<sup>[28]</sup>

Whatever the mechanism, the diversity imparts the lattice-invariant deformation (LID) associated with the relaxation of martensite's homogenous shape change into an invariant plane strain (IPS).<sup>[29]</sup> In Fe-29.6wt pctNi, the dislocation-assisted LID, typical in lath martensites, is observed over the range of temperatures (264 K to 253 K), where the variation of  $\phi^K$  is characterized by an apparent activation energy ( $1.8 \times 10^{-19}$  J/event) compatible with dislocation processes. The

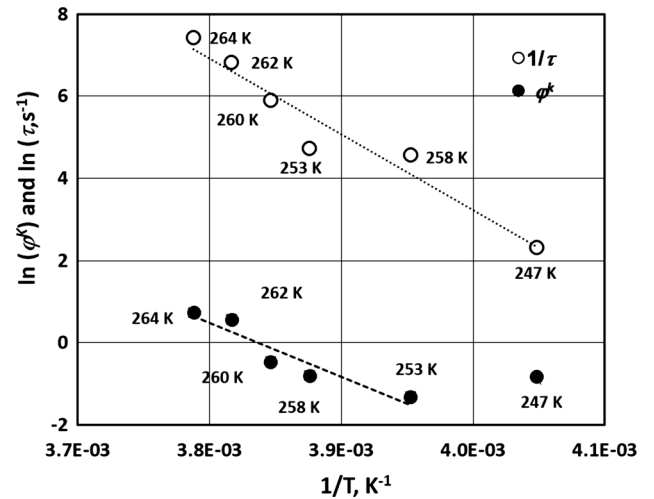


Fig. 2—Arrhenius graphs. Values of  $\phi^K$  and  $1/\tau$  typical of Fe-29.6 wt pct Ni isothermally transformed at the reaction temperatures in the labels.

twinning-assisted LID predominates below 253 K, yielding internally twinned plate martensites that form very fast and tend to run across the austenite grains, as well as forming autoaccommodated (anti-thermal) chain reactions that feedback elastic free energy.<sup>[30]</sup> Notably, the LID transition coincides with the observation of the initial transformation burst in Fe-29.6 wt pct Ni.<sup>[20]</sup> The autoaccommodated twinned martensite units that compose such bursts explain the increasing values of  $V_{VM0}$  at  $T < 253$  K—see Table I.

## V. NUCLEATION BARRIER

To calculate the activation energy for martensite nucleation,  $\Delta W_a$ , we assumed a single thermally activated barrier. The probability of *initial martensite nucleation* is given by the ratio  $(\nu\tau)^{-1}$ , where  $\tau$  is the incubation factor and where  $\nu$  is a frequency factor that depends on the nucleation mechanism.<sup>[31]</sup>

$$(\nu\tau)^{-1} = P_n(T) \exp\left(-\frac{\Delta W_a}{k_B T}\right), \quad [8]$$

where  $k_B$  is the Boltzmann's constant, and  $P_n(T)$  is the probability of existing nucleation loci for initiating the reaction at temperature  $T$ . Recalling Guimarães and Rios,<sup>[32]</sup>

Table I. Zero External Field—Eq. [9] Fitting Parameters

$T$ , K	$\phi^K$	$\tau$ , s	$V_{VM0}$	$R^2$	$\Delta W_a$ , J/Event
264	2.10E+00	1.68E+03	2.56E-03	0.99	1.28E-19
262	1.70E+00	9.19E+02	2.97E-05	0.99	1.26E-19
260	6.30E-01	3.66E+02	2.10E-02	0.95	1.22E-19
258	4.50E-01	1.14E+02	5.04E-02	0.91	1.18E-19
253	2.70E-01	9.63E+01	7.62E-02	0.86	1.16E-19
247	4.40E-01	1.01E+01	2.64E-03	0.94	1.07E-19
77	4.00E-01	2.03E+00	1.15E-02	0.98	—

$$P_n(T) = \frac{\Delta S(T^* - T)}{k_B T}, \quad [9]$$

where  $T^*$  is the highest temperature at which an austenite defect is capable of sustaining in the presence of thermal agitation, correlated with atomic groups compatible with the nucleation path.  $\Delta S$  is the entropy change. Substituting Eqs. [9] into [8],

$$(\nu\tau)^{-1} = \frac{\Delta S(T^* - T)}{k_B T} \exp\left(-\frac{\Delta W_a}{k_B T}\right). \quad [10]$$

Since  $T^*$  cannot be obtained directly from the transformation curve, we fit  $T^*$  to describe the temperature dependence in  $\tau$  compatible with Eq. [10]. A fitting correlation  $R^2 = 0.91$  was obtained with  $T^* = 270$  K, which is slightly above the temperature of the sluggish reaction shown in Figure 1. Next, we inserted that value of  $T^*$  into Eq. [10] to calculate the values of  $\Delta W_a$  shown in Table 1. Remarkably, these energies duplicate the classical linear dependence of  $\Delta W_a$  on the chemical driving force<sup>[33–35]</sup> down to 247 K, bursts included—see Figure 3. Caveat: we used  $\nu = 10^{14} \text{ s}^{-1}$  to compare with the values of  $\Delta W_a$  in Reference 20 although a lower frequency should be more appropriate.<sup>[34]</sup> We attribute the difference between the slopes of the charts in Figure 3 to the differences in the underlying formalisms.

## VI. MARTENSITE BURST TRANSFORMATION

The martensite burst is a notable event signaled by sonic emission and heat evolution<sup>[36]</sup> that yield significant volume fractions of martensite. The first nucleation event in a grain may suffice to trigger a burst.<sup>[37]</sup> Such transformation bursts, where each unit serves as nucleation locus for the next event, are typically autocatalytic.

The fact that an apparently time-independent transformation burst, the size of which increases with increasing chemical driving force, precedes a time-dependent (thermally activated, isothermal) transformation tails poses a conundrum: is the burst a fast

isothermal (thermally activated) transformation<sup>[37]</sup> or a mechanical autocatalytic event? To explore this matter further, observe the chart in Figure 4. This figure shows that at high temperatures,  $\phi^K$  varies proportionally to  $\tau$ . However, around the martensite-start temperature of Fe-29.6 wt pct N, 253 K, there is an abrupt change in the chart. Below 253 K,  $\phi^K$  becomes near-invariant, while the grains are transformed by autocatalytic chains comprising twinned martensite. Thus, we may associate the resultant microstructure variation to changes in the LID. Moreover, because the intergrain spread of the martensite burst bears thermal activation—Figure 3 of Reference 38—it is apparent that thermally activated and anti-thermal components are present in the martensitic transformation burst.

## VII. MAGNETIC-ASSISTED MARTENSITE TRANSFORMATION

Korenko also has discussed magnetic-assisted martensitic transformation in his book.<sup>[20]</sup> Such data relevant to the validation of Eq. [7] are shown in Figures 5 and 6. The dashed lines demonstrate the high fitting correlations ( $R^2 > 0.90$ ) obtained based on magnetic-assisted martensite in Fe-29.6 wt pct Ni. The fitting parameters are given in Table II. Inspection of these charts indicates that the magnetic field promoted martensite transformation even above  $T^*$ (253 K). However, the size of the initial burst induced by 90 kOe increases from 17 pct at 282 K to 70 pct at 271 K, despite the higher thermal energy ( $k_B T$ ) available to assist the time-dependent transformation tails at 282 K.<sup>[20]</sup> This finding suggests that thermal energy somehow would interfere with the effect of the magnetic field.

To check this possibility, we assumed influence of the magnetic field on the probability of existing nucleation loci to initiate the transformation. *Ad hoc*,  $P_n(T) = \frac{\Delta G_m}{k_B T}$ , where  $\Delta G_m$  is a magnetic driving force. Thus, recasting Eq. [10],

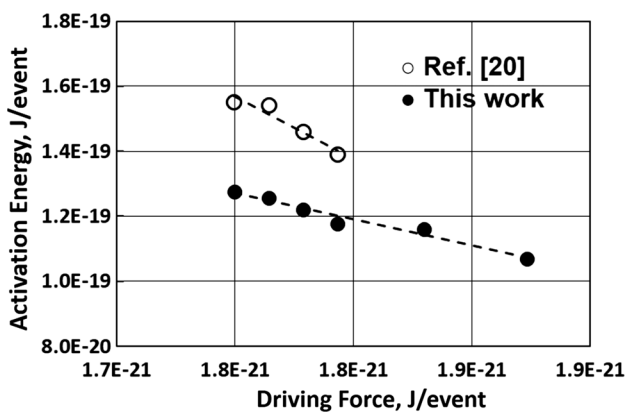


Fig. 3—Activation energy for martensite nucleation as a function of the driving force: filled circle—calculated with Eq. [10]. Open circle—reported in Ref. [20].

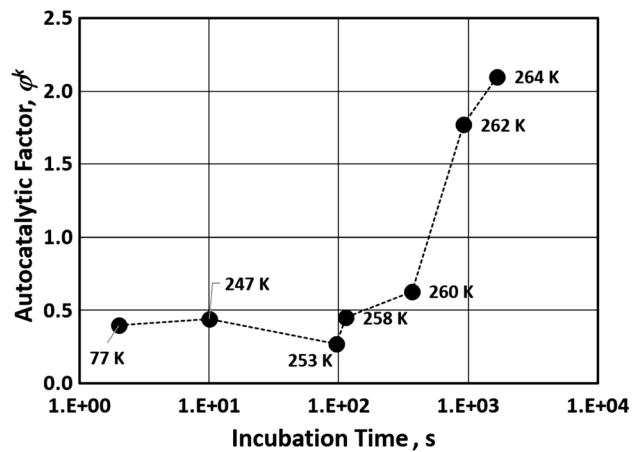


Fig. 4—Comparison of the values of  $\tau$  and  $\phi^K$  obtained by fitting the transformation curves with Eq. [7]. The labels show the reaction temperatures.



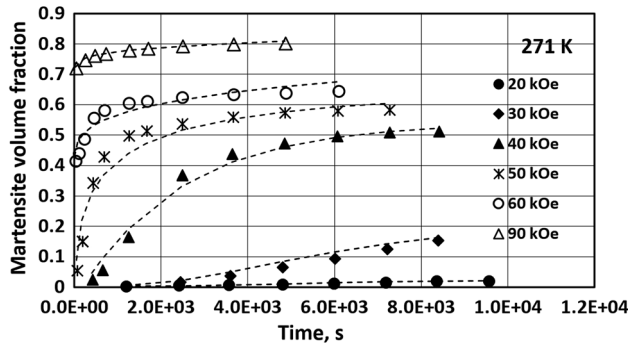


Fig. 5—Magnetic-assisted, isothermal martensite transformation curves, Eq. [7]. Fe-29.6 wt pct Ni at 271 K, data reported in Ref. [20].

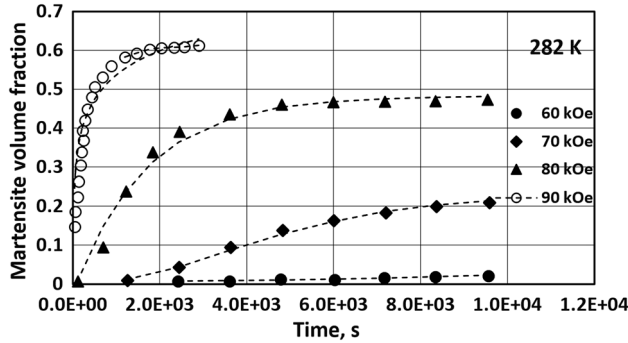


Fig. 6—Magnetic-assisted, isothermal martensite transformation curves, Eq. [7]. Fe-29.6 wt pct Ni at 282 K, data reported in Ref. [20].

Table II. Magnetic-Assisted Martensite—Eq. [9] Fitting Parameters

Field, kOe	$\varphi^K$	$\tau$ , s	$V_{VM0}$	$R^2$
271 K				
20	2.10E+00	1.07E+03	3.17E-04	0.94
30	1.77E+00	1.07E+03	1.20E-03	0.99
40	1.00E+00	2.79E+02	4.98E-02	0.98
50	5.00E-01	4.35E+01	6.66E-02	0.94
60	2.50E-01	7.27E+00	5.13E-02	0.83
90	2.80E-01	2.28E+01	1.78E-02	0.99
282 K				
60	2.00E+00	2.17E+03	8.96E-04	0.96
70	1.50E+00	1.11E+03	4.66E-03	0.99
80	1.00E+00	8.34E+01	5.49E-03	0.98
90	2.50E-01	3.92E+01	1.29E-01	0.60
140	3.20E-01	2.59E+01	1.06E-02	0.94

$$(\nu\tau)^{-1} = \frac{\Delta G_m}{k_B T} \exp\left(-\frac{\Delta W_{am}}{k_B T}\right). \quad [11]$$

Using the values of  $\Delta G_m$  tabulated in Korenko's book,<sup>[20]</sup> and those of  $\tau$  in Table II, we obtained the scatter plot in Figure 7. For comparison, data typical of the martensite transformation under zero-field are included. Simple inspection of the chart indicates that a common straight line would describe the three datasets

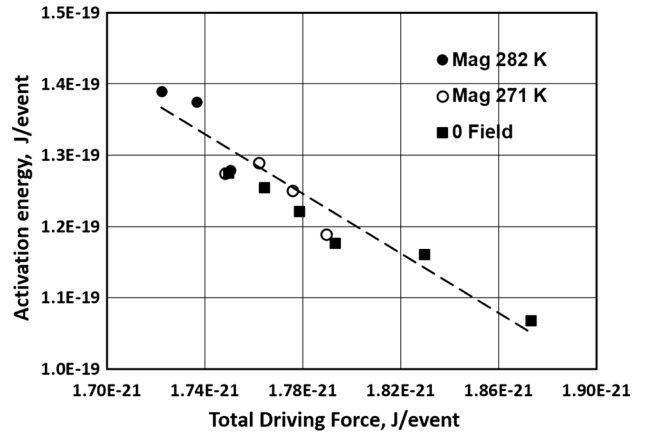


Fig. 7—Activation energy for martensite nucleation as a function of the driving force. Zero-field transformation, Eq. [10], and magnetic-assisted transformation, Eq. [11].

(fitting correlation,  $R^2 = 0.93$ ). Therefore, we conclude that the magnetic field appears to influence the stability of the correlated atomic groups that access the nucleation path, a topic that deserves further investigation.

## VIII. APPLICABILITY OF THE MODEL BEYOND CURRENT WORK

The approach to the martensite transformation curve described in the foregoing has been successfully applied to FeNiC<sup>[17]</sup> and FeNiMn<sup>[7]</sup> alloys and to FeC steels.<sup>[18]</sup> We believe the model could be applied to other systems, as well. To reinforce this assertion, Figure 8 demonstrates the fitting of martensite transformation curves with a high fitting coefficient. This martensite originates from a metastable austenite of a “18Cr-8Ni” stainless steel with different carbon concentrations transformed by cryogenic cooling recently reported by Masumura *et al.*<sup>[39]</sup> We show in Figure 8 that these researchers'

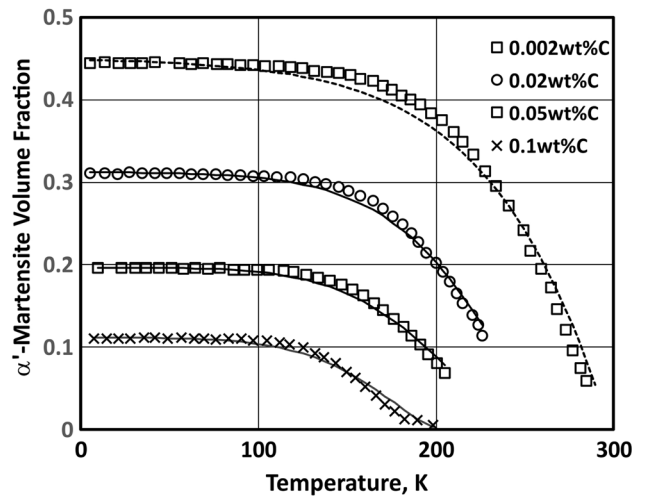


Fig. 8—Transformation curves typical of martensite transformation in “18Cr-8Ni” steels induced by cryogenic cooling, fitted with Eq. [6]. Data from Ref. [39].

**Table III. Cryogenic-Cooled 18Cr-Ni Steel<sup>[39]</sup>**

Weight Percent	$T^*$	$\phi^K$	$V_{VM0}$	$R^2$
0.002	299	1.06	1.28E-02	0.98
0.020	266	1.40	2.98E-03	0.99
0.050	254	1.70	7.15E-03	0.99
0.100	199	1.40	4.38E-03	0.98

curves fitted with our model. The fitting parameters are shown in Table III.

## IX. SUMMARY AND CONCLUSIONS

The high fittings of experimental transformation curves considered in the present work warrant the proposed model for the martensite transformation curve. The usefulness of the model Eq. [5] derives from consideration of the probabilistic aspect of the microstructure evolution, which avoids the complication inherent to the sequence of martensite unit formation, as well as from the utilization of a kinetic equation that acknowledges the generally accepted autocatalytic and nucleation-controlled aspects of martensite transformation. The model acknowledges that although thermodynamic principles determine the possibility of the transformation microstructure, the fraction transformed is determined by the accommodation of the transformation strains in the environment where the martensite units form.<sup>[16]</sup> Notably, the analysis of the fitting parameters in Eq. [5] provides expeditious clues about the reaction kinetics. The values of  $\tau$  obtained from the referenced alloy reiterated the classical linear dependence of  $\Delta W_a$  on the driving force that characterizes martensite kinetics.<sup>[33–35]</sup> To summarize, despite simplifications common to phenomenological/formal models, the description of the martensite transformation curve consolidated into Eq. [5] is considered operational. Furthermore, the model is expected to be applicable to martensite in other systems, and it is shown to fit recent data<sup>[39]</sup> on “18Cr-8Ni” stainless steel.

## ACKNOWLEDGMENTS

P.R. Rios is grateful to Conselho Nacional de Desenvolvimento Científico e Tecnológico, CNPq and to Fundação de Amparo à Pesquisa do Estado do Rio de Janeiro, FAPERJ for financial support.

## REFERENCES

1. W.J. Harris and M. Cohen: *Trans. AIME*, 1949, vol. 180, pp. 447–70.
2. D.P. Koistinen and R.E. Marburger: *Acta Metall.*, 1959, vol. 7, pp. 59–60.
3. V. Raghavan and A.R. Entwisle: *Physical properties of martensite and bainite, ISI Spec Rep 93*, Iron and Steel Institute, London, 1965, pp. 30–37.

4. M. Lin, G.B. Olson, and M. Cohen: *Metall. Trans. A*, 1992, vol. 23, pp. 2987–97.
5. T. Kakeshita, T. Fukuda, and T. Saburi: *Sci. Technol. Adv. Mater.*, 2000, vol. 1, pp. 63–72.
6. S.J. Lee and Y.K. Lee: *Acta Mater.*, 2008, vol. 56, pp. 1482–90.
7. S.M.C. Van Bohemen and J. Sietsma: *Mater. Sci. Technol.*, 2009, vol. 25, pp. 1009–12.
8. S.J. Lee and C.J. van Tyne: *Metall. Mater. Trans. A*, 2012, vol. 43A, pp. 422–27.
9. F. Huyan, P. Hedström, A. Borgenstam: *Proceedings 2S of the International Conference on Martensitic Transformations, ICOMAT-2014, Materials Today*, 2015, pp. S561–S564.
10. Z. Dai, R. Ding, Z. Yang, C. Zhang, and H. Chen: *Acta Mater.*, 2018, <https://doi.org/10.1016/j.actamat.2018.04.040>.
11. L. Liu, B.B. He, G.J. Cheng, H.W. Yen, and M.X. Huang: *Scripta Mater.*, 2018, vol. 150, pp. 1–6.
12. A.J. Markworth and M.L. Glasser: *J. App. Phys.*, 1983, vol. 54, p. 3502, <https://doi.org/10.1063/1.332416>.
13. D. E. Laughlin, N. J. Jones, A. J. Schwartz, T. B. Massalski: *ICOMAT-08*, G.B. Olson, D.S. Lieberman, and A. Saxena, eds., TMS (The Minerals, Metals & Materials Society), 2009, pp. 141–43.
14. M. Villa and M.A.J. Somers: *Scripta Mater.*, 2018, vol. 142, pp. 46–49.
15. J.R.C. Guimarães and P.R. Rios: *J. Mater. Res. Technol.*, 2018, <https://doi.org/10.1016/j.jmrt.2018.04.007>.
16. O. Kastner and G.J. Ackland: *J. Mech. Phys. Sol.*, 2009, vol. 57, pp. 109–21.
17. J.R.C. Guimarães and J.C. Gomes: *Acta Metall.*, 1978, vol. 26, pp. 1591–96.
18. G. Ghosh and V. Raghavan: *Mats. Sci. Eng. A*, 1986, vol. 80, pp. 65–74.
19. G. Krauss and A.R. Marder: *Metall. Trans.*, 1971, vol. 2, pp. 2343–57.
20. K. Korenko: DSc. thesis, Massachusetts Institute of Technology, Cambridge, Massachusetts Martensitic in High Magnetic Fields, 1973.
21. R.E. Cech and D. Turnbull: *Trans. AIME*, 1956, vol. 206, pp. 124–32.
22. M. Cohen and G.B. Olson: *Suppl. Trans. JIM*, 1976, vol. 17, pp. 93–98.
23. J.R.C. Guimarães and A. Saavedra: *Mater. Sci. Eng.*, 1984, vol. 62, pp. 11–15.
24. V. Raghavan: *Acta Metall.*, 1969, vol. 17, pp. 1299–03.
25. S. Morito, X. Huang, T. Furuhara, T. Maki, and N. Hansen: *Acta Mater.*, 2006, vol. 54, pp. 5323–21.
26. A. Shibata, S. Morito, T. Furuhara, and T. Maki: *Acta Mater.*, 2009, vol. 57, pp. 483–92.
27. R.G. Davies and C.L. Magee: *Metall. Trans.*, 1970, vol. 1, pp. 2927–31.
28. M. Grujicic and G.B. Olson: *Interface Science*, 1998, vol. 6, pp. 155–64.
29. M.S. Wechsler, D.S. Lieberman, and T.A. Read: *Trans. AIME*, 1953, vol. 197, pp. 1503–15.
30. R.F. Bunshah and R.F. Mehl: *Trans. AIME*, 1953, vol. 197, pp. 1251–58.
31. C.H. Shih, B.L. Averbach, and M. Cohen: *Trans. AIME*, 1955, vol. 203, pp. 183–87.
32. J.R.C. Guimarães and P.R. Rios: *J. Mater. Sci.*, 2008, vol. 43, pp. 5206–10.
33. L. Kaufman and M. Cohen: *Prog. Metal Phys.*, 1958, vol. 7, pp. 165–46.
34. G. Ghosh and G.B. Olson: *Acta Metall.*, 1994, vol. 42, pp. 3371–79.
35. K. Wang, S. Shang, Y. Wang, Z. Liu, and F. Liu: *Acta Mater.*, 2018, vol. 147, pp. 261–76.
36. E.S. Machlin and M. Cohen: *Trans. AIME*, 1951, vol. 191, pp. 1019–27.
37. A.R. Entwisle: *Metall. Trans.*, 1971, vol. 2, pp. 2397–07.
38. J.R.C. Guimarães and P.R. Rios: *Mat. Res.*, 2017, vol. 20, pp. 1548–53.
39. T. Masumura, T. Tsuchiyama, T. Takaki, T. Koyano, and K. Adachi: *Scripta Materialia.*, 2018, vol. 154, pp. 8–11.